ELSEVIER

Contents lists available at ScienceDirect

Journal of Constructional Steel Research

journal homepage: www.elsevier.com/locate/jcsr



Response of stainless steel beam-to-column bolted connections under column removal[☆]

Weiran Li a,*, Manuela Cabrera b, Marios Theofanous b, Sheida Afshan a

ARTICLE INFO

Keywords:
Progressive collapse
Robustness
Stainless steel connection
Ductility
Fracture modelling

ABSTRACT

This study presents a comprehensive numerical investigation comparing the performance of stainless steel and carbon steel beam-to-column connections under static and dynamic column removal scenarios, aiming to assess the potential of stainless steel to enhance structural robustness through increased connection strength and ductility. Validated finite element models of two connection types, web angle (WA) and top and seat with web angle connections (TSWAC), were used to assess connection performance under static and dynamic column removal scenarios, considering variations in angle cleat thickness, bolt material, and boundary conditions. The results show that adopting stainless steel in key connection components significantly enhances both the strength and ductility of the connection, thereby improving the overall structural robustness. The maximum bending moment increased by a factor of 1.3 to 2, while the maximum loading capacity under column removal scenario improved by 1.5 to 2 times. In dynamic scenarios, stainless steel connections exhibited lower peak displacements (\sim 20 %) and improved energy absorption, with dynamic increase factors may exceeding code-recommended values. These finding evidence the potential of targeted stainless steel use to enhance resistance against progressive collapse, with a minor and relatively inexpensive structural intervention.

1. Introduction

Within the context of Eurocode [1], robustness is defined as the ability of a structure to withstand events like fire, explosions, impact, or the consequence of human error without being damaged to an extent disproportionate to the original cause. Hence, structures designed and constructed to have robustness should not suffer from disproportionate collapse. Notable examples of structural failures due to disproportionate collapse include the Ronan Point in London (1968) and the Champlain Towers in Miami (2021). In these cases, failure was caused by the onset of initial localised damage to a few structural components which then gradually spread and ultimately resulted in the collapse of the entire structure or a significant portion of it [2-4]. Current international structural design codes require measures to prevent disproportionate collapse under accidental loading. For steel and composite frames under such loads, the spread of initial damage can be prevented through the provision of alternative load paths to redistribute the loads previously resisted by the failed structural components, such as columns. These paths are generally realised through load-carrying mechanisms such the catenary action of the floor beams and the membrane action of the floor slabs, all of which rely heavily on the load-carrying capacity and ductility of the beam-to-column connections in the vicinity of the localised damage, which are subjected to high strength and ductility demands.

Notional column-loss analysis is commonly employed in structural design codes [5–7], as well as in experimental testing and numerical modelling studies of steel framed structures, to assess robustness. This method is based on the assumption that the removal of a column simulates the strength and ductility demand imposed on the frame system in case of a localised failure of a structural element and tests its ability to transfer the loads previously supported by the compromised column to the adjacent structural elements. Although the real column loss scenario impacts the overall structural behaviour, simplified idealizations can be used in such analysis. Izzuddin et al., [8] suggested that evaluating the performance at full structural level can be achieved by modelling the sub-structural responses in detail. This approach enables researchers to focus on the affected single layer compartment rather than the entire structure while capturing interactions with surrounding structures

E-mail address: wl2u20@soton.ac.uk (W. Li).

^a Faculty of Engineering and Physical Sciences, University of Southampton, UK

^b School of Engineering, University of Birmingham, UK

^{*} This article is part of a Special issue entitled: 'High performance steel' published in Journal of Constructional Steel Research.

^{*} Corresponding author.

through appropriate boundary conditions. Therefore, studying the column removal mechanism can be significantly simplified by focusing on the structure near the removed column, including the column and the two adjacent beams [9]. Ensuring the integrity of the beam-to-column connections in the vicinity of the removed column is key for robustness, it allows catenary action to develop and alternative load paths to be exploited.

While sub-structural modelling provides an efficient and widely accepted means of assessing robustness under localised failure, some researchers have pursued full-structure modelling to capture global collapse mechanisms and system-wide interactions more comprehensively. One example is the 20-storey benchmark building developed by Huang et al. [10], which includes floor slab composite action and aims to standardise progressive collapse analysis at the whole building scale. However, the high computational cost and complexity of such large-scale models limits their practicality for detailed parametric investigations or studies focusing on material-level behaviour. Furthermore, these models are typically based on carbon steel and do not explore the potential benefits of alternative materials with superior mechanical properties.

In steel framed structures, highly ductile bolted beam-to-column connections have emerged as a promising solution to mitigate progressive collapse [11–13]. This approach aims to maximise the vertical load carrying capacity provided by the beam catenary action [14], confining the damage within the bays and stories adjacent to the damaged column. Over the past few decades, researchers have extensively studied the performance of structural systems subjected to column removal scenarios and the subsequent development of catenary action via both experimental testing [15-20] and numerical modelling [21-26]. However, these studies have primarily focused on carbon steel. While effective, carbon steel has limitations in terms of ductility and strainhardening behaviour, particularly under large deformations and elevated temperatures. In contrast, research on stainless steel connection components remains relatively limited. Stainless steel materials are naturally suited to contribute to achieve the required tie resistance and rotation capacity due to their inherent high ductility, strain-hardening and fire protection characteristic [27-30]. More recently, a series of high-strength stainless steels [31-33] have been introduced, revealing their significant potential as critical connection components.

In the scope of this work, a comprehensive three-dimensional finite element model was developed to assess the mechanical behaviour of stainless steel connection components in a column removal scenario. The model was validated through simulations of stainless steel beam-to-column connections under static loading and carbon steel column removal experiments. A full range of material parameters was compiled involving the fracture behaviour of some key materials, ensuring both accuracy and computational efficiency of the finite element model. Additionally, parametric studies were carried out to investigate the impact of connection type, material grade and angle cleat thickness on the static and dynamic responses during a column removal scenario. The obtained results and analysis and discussions thereof are presented hereafter.

2. Validation of numerical models

2.1. Available test results

The results of stainless steel bolted beam-to-column connection tests conducted by Elflah et al., [31], and the carbon steel two-sided bolted beam-to-column connection tests conducted by Yang et al., [20] were used to validate the finite element (FE) model developed herein. This section presents an overview of the key details of the two experimental programmes for the FE model development. A series of stainless steel bolted beam-to-column connection cantilever tests were conducted by Elflah et al., [31] at the University of Birmingham. The study reported, for the first time, the results of full-scale tests on stainless steel beam-to-

column bolted connections under static monotonic loading and included four types of bolted connections: Top and Seat Angle Cleat (TSAC), Top and Seat with Web Angle Cleat (TSWAC), Extended End Plate (EEP) and Flush End Plate (FEP). In this paper, validation of only the first two connection types, TSAC and TSWAC are considered. The beams and columns used were both built up welded I-240 \times 120 \times 12 \times 10 for all tests. The angle cleat sections used in the TSAC and TSWAC tests were all L100 \times 100 \times 8. The beams, columns and angle cleats were all austenitic EN 1.4301 stainless steel and the bolts were fully threaded M16 austenitic A4–80 stainless steel.

A series of two-sided bolted beam-to-column connection tests were conducted at Nanyang Technological University to investigate the behaviour of different types of carbon steel bolted beam-to-column connections as reported by Yang et al., [20]. The aim of these tests was to determine the ability of the considered beam-to-column connections to deform under catenary action and understand their failure modes. In total, five different types of bolted carbon steel beam-tocolumn joints were investigated, representing pinned, semi-rigid and rigid connections. These included Web Angle (WA), Top and Seat Angle Cleat (TSAC), Top and Seat with Web Angle Cleat (TSWAC), Flush End Plate (FEP) and Extended End Plate (EEP) connections. This paper focuses on the validation of the WA and the TSAC [20] connections. A twosided beam-to-column connection setup was used. Each specimen consisted of two steel beams and a steel column. The column was S355 $\text{UC203} \times \text{203} \times \text{71}$ and the beams were S355 UB254 \times 146 \times 37 for all specimens. The angle cleats were S275 L90 \times 90 \times 8 and the bolts were grade 8.8 fully threaded M20 for all specimens. The tests were conducted by applying a downward displacement to the column using an actuator, allowing for the development of arching action and catenary action and their effects on beam-to-column connection response via restraining the inward movement of the beam ends. The selected connection configurations (TSWAC, TSAC, and WA), included in Annex C of EN 1993-1-8 (2024) [34], represent commonly used connection types in structural steel practice and offer available experimental data for both carbon steel and stainless steel, enabling robust validation of the numerical models.

2.2. Material modelling for connection model validation

For the carbon steel connection tests, stress-strain models were developed to simulate the material behaviour of the beam-to-column connection components. The quad-linear model proposed by Yun and Gardner [35] for modelling the stress-strain behaviour of carbon steel, together with the key material parameters provided in Table 1 were used to obtain the engineering stress-strain curves, up to the pre-necking

Table 1Summary of key material properties used in the development of stress-strain models for validation.

Connection part	Е	fy	$f_{ m u}$	ε_{u}	$arepsilon_{ m f}$	n	n' _{0.2,}
	(MPa)	(MPa)	(MPa)	(%)	(%)		
S275 angle cleat	210,000	275	430	21.63	27	-	-
S355 beam/ column	210,000	355	490	16.53	-	-	-
8.8 M20 bolt fully threaded	207,000	680	966	6.00	8.2	-	-
EN 1.4301 beam/column flange	196,500	248	630	60.00	66	5.20	2.37
EN 1.4301 beam/column web	205,700	263	651	62.00	65	6.70	2.41
EN 1.4301 angle cleat	197,600	280	654	50.00	55	12.2	2.49
A4–80 M16 fully threaded bolt	191,500	617	805	-	-	17.2	3.68

stage, for the S355 beam and column and the S275 angle cleat components. The adopted quad-linear model reflects the characteristics of yield platform, strain hardening and ultimate stress of hot rolled carbon steel. In the absence of material data for grade 8.8 M20 fully threaded bolts, the tensile stress-strain data reported by Song et al., [33] was used. For the stainless steel connection tests, the two-stage Ramberg-Osgood model [36,37], commonly used in nonlinear stress-strain materials, was used to model the stress-strain behaviour of the bolted beam-to-column connection components - namely, the beam, column, angle cleat and bolt – up to the pre-necking stage, based on the key material parameters measured and reported in Table 1. The material parameters in Table 1 are the Young's modulus E, the yield stress f_v , taken as the 0.2 % proof stress for stainless steel, the ultimate tensile stress f_u , the strain corresponding to ultimate tensile stress ε_u , strain at fracture ε_f and two-stage Ramberg-Osgood model strain-hardening exponents n and $n'_{0,2,11}$ reported by Elflah et al., [38]. According to [38], the TSAC and TSWAC tests were terminated before the complete fracture of the bolts, hence their stress-strain responses were only modelled up to the necking stage. In the carbon steel connection testes reported in [20], failure occurred by fracture of the S275 angle cleats; therefore fracture was modelled using the void growth model (VGM) model [39-41], as described in Section 3.3.

2.3. Numerical model development

This section presents the development and validation of the finite element (FE) models for the steel and stainless steel beam-to-column bolted connection tests presented in Section 2.1. The general purpose FE modelling software ABAQUS [42] was used to create the numerical models. The geometry of the models was created in SolidWorks [43], adopting the measured geometric dimensions of the tested specimens, which was then imported into ABAQUS [42] as an assembly. The fully threaded A4-80 M16 and grade 8.8 M20 bolts were simplified as smooth cylinders with an area equal to the stress area A_s of the real bolt, which is a commonly adopted approach for modelling of threaded bolts [33,38,44], the bolt hole diameter was correspondingly reduced to ensure a bolt-to-hole edge distance of approximately 1 mm in accordance with the clearance hole diameter exceeding the bolt diameter by 2 mm. The bolt head and nut were also simplified as integral cylinders with the bolt shank, as bolt striping failure was not of concern. On the other hand, the washer was considered separately to ensure that the nut did not experience abnormal mesh deletion. The full geometry of the

cantilever beam-to-column connection tests and half of the length of the two-sided bolted beam-to-column connection tests, with suitable symmetry boundary conditions, were modelled. Contact between the various connection parts was defined using the 'General Contact' command provided by ABAQUS [42]. The contact property consisted of a 'hard contact' in the normal direction, and a 'penalty' in the tangential behaviour, with a friction coefficient of 0.3.

The boundary conditions at the beam and column ends were defined such as to mimic the test conditions; a schematic representation is shown in Fig. 1. For the stainless steel connection models, the boundary conditions at both the beam and column ends were defined on reference points to which the degrees of freedom of the specimen's end sections were coupled. All degrees of freedom of the bottom of the column were fully restrained, while the top of the column, only the translational degrees of freedom were fixed. The beam end was loaded via displacement control in the y-axis direction. For the two-sided bolted beam-column connection test models, accurately defining the boundary conditions at the beam ends is crucial for reproducing the arching action and catenary action effect in FE models. At the beam ends, all displacement degrees of freedom were restrained (i.e., $U_x = U_y = U_z = 0$), thus simulating the restraint provided by the A-frame and the reaction wall in the tests. Additionally, rotations UR_v and UR_z were restrained, while URx was left free to simulate the pinned ends.

All the modelled components were meshed using the C3D8R element, which is a general-purpose linear brick element with reduced integration. As recommended in [44,45], at least three layers of elements were used to mesh the thickness of critical components, such as bolts, angles and the beams, to avoid hourglass effects and shear locking. A mesh sensitivity analysis was carried out to establish suitable mesh sizes for the modelled connections components. The mesh sizes were selected to accurately capture the response of the models while minimizing computational time. For the beam and column members, global mesh sizes of 10 mm and 15 mm, respectively, were used. Using a coarse mesh for the beams and columns is justified by the fact that the beams and columns generally remained elastic throughout the tests. In contrast, the bolt, which exhibits complex mechanical behaviour and potential failure, was meshed with the smallest element size employed herein of 2.5 mm. Similarly, a 2.5 mm mesh size was used for the potential fracture zone (i.e., the corner region) of the angle cleat sections, while a larger mesh size of 5 mm was used for the remainder of the section to reduce computational effort. The dynamic explicit solver was used for all simulations, to allow fracture and lost contact to be

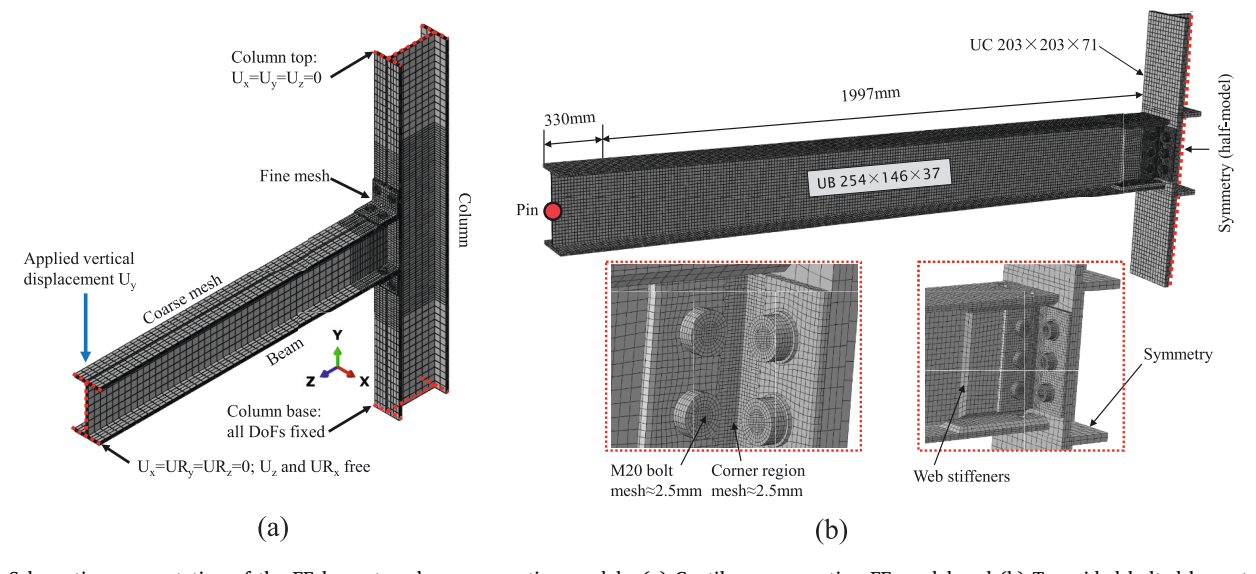


Fig. 1. Schematic representation of the FE beam-to-column connection models. (a) Cantilever connection FE model and (b) Two-sided bolted beam-to-column connection FE model.

simulated without convergence issues. Quasi-static response was obtained by ensuring that the kinetic energy remained less than 1 % of the internal energy throughout the loading process in all models.

2.4. Numerical model validation results

For the stainless steel bolted connections, the moment-rotation curves obtained from the FE simulations and the tests are compared in Fig. 2(a) and (b). Moment was determined as the product of the applied force at the beam end and the beam length, and rotation was determined as the joint rotation, which does not take into account the deformation of the beam. As shown, the models were capable of replicating the measured moment-rotation behaviour of the connections over the full response range including the initial stiffness, peak load and rotation capacity with a good degree of predictive accuracy ($R^2 = 0.988-0.994$). The models were also capable of accurately simulating the test failure modes, with the bolt failure modes and the failure locations of the FE models being consistent with the observations from the tests, as shown in Fig. 2(a) and (b). Fig. 2(c) and (d) compare the test and FE vertical load versus vertical column displacement of the modelled two-sided bolted beam-to-column connection tests. The FE models were capable of accurately replicating the measured force-displacement behaviours over the full response range, including initial stiffness, maximum load and fracture ($R^2 = 0.954-0.977$). The test and FE failure modes are also shown in Fig. 2(c) and (d), where the sever plastic deformation of the bolted angle cleats and the bolts is seen to be accurately captured, whereas the angle corner fracture on the column side of the web angle connection and the bottom angle corner fracture of the top and seat angle connection, are also correctly simulated.

3. Parametric study model development

3.1. Structural frame and loading scenarios

Using the FE models validated in the previous section, extensive parametric studies were conducted to assess the response of beam-tocolumn connections joining carbon steel beams and columns. The primary focus was on the single-story bare steel beam-to-column connection, with the fundamental approach involving assessing the idealized performance of the overall structure through modelling of the repeating units. However, the selection and simplification of these repeating units must consider their interaction with the surrounding steel frame, necessitating the use of appropriate boundary conditions. The adopted frame layout is shown in Fig. 3, with beam spans of 8 m and floor heights of 3 m. Each half-span considered for the column removal scenario exhibits symmetric structural behaviour, hence a 4 m long beam was considered. The boundary condition at the beam end can be simplified as a roller support allowing the beam to pull in at high deformations, with the addition of an axial spring, with suitable axial stiffness K_A , to simulate the axial restraint provided by the surrounding frame structure. Three levels of axial restraint stiffness were considered, namely full restraint ($K_A = \infty$), partial restraint ($K_A = 67.5 \text{ kN/mm}$) and no restraint (cantilever model $K_A = 0$). The models without axial restraint were used to obtain the moment-rotation response and the classification of the parametric beam-to-column connection models in absence of a coexisting tensile force. The value of the partial constraint stiffness $K_A = 67.5$ kN/mm was determined based on the linear elastic plane frame analysis of the surrounding frame shown in Fig. 3. The parametric models had a relatively short column length which is considered suitable for this application, since the pinned and semi-rigid connections used will not result in significant bending or deformation of the column.

Figure 4 depicts a quarter-beam-column connection model developed for the purpose of the parametric study, where symmetry boundary conditions were applied to restrict the displacements and rotational DOFs along the symmetry planes. The loading and boundary conditions were as previously described for the validation models, with the

exception of the addition of the linear axial spring at the beam end to simulate the axial restraint stiffness [29]. The partial and full restraint models were investigated under two column removal scenarios: static and dynamic column removal. In the static column removal case, the column was loaded quasi-statically, while in the dynamic column removal models, the effect of removing the column after the application of uniformly distributed beam loads was investigated. The dynamic models also considered the gravitational field, with a magnitude of 9800 mm/s². Four additional mass boxes were included to simulate the uniform loading on the beam, as shown in Fig. 4. These were connected to the bottom centre of the beam using 'Tie' constraint, and the density was adjusted to simulate two load cases of 10 kN/m and 20 kN/m. The applied uniform distributed load (UDL) was selected to ensure connection failure and facilitate the assessment of progressive collapse resistance. While the exact UDL depends on design loads, beam spacing and overall building layout, the chosen values of 10 kN/m and 20 kN/m are representative of accidental loading scenarios in typical office or residential buildings. For example, with a dead load $g = 3 \text{ kN/m}^2$, a live load $q = 2kN/m^2$, a load combination factor $\psi_1 = 0.5$ and a column spacing of 5.7 m, this results in approximately 10 kN/m for a perimeter sub-frame and 20 kN/m for an internal sub-frame.

The remaining parts had a fixed density of 8E-9 ton/mm³. Damping was modelled using the widely used Rayleigh damping approach available in Abaqus [42]. A representative damping ratio $\zeta=5$ % was assumed [46], which together with the natural frequency of the system, obtained from a modal analysis, was used to determine the mass proportional damping coefficient α_R which was then added to the material properties. The dynamic models involved two analysis steps; in step 1, the downward gravity force, to simulate the weight of the specimen and the beam UDL was applied until the system reached equilibrium, while a fully fixed boundary condition was assigned to the column top, and in step 2, the vertical displacement boundary condition at the column top was removed instantly to simulate the sudden column removal scenario.

3.2. Beam-to-column connection configurations

The parametric study focused on two connection configurations including web angle (WA) and top and seat with web angle (TSWAC), representing nominally pinned and semi-rigid connections, respectively. These two types of angle connections were selected as they possess relatively high rotation capacity, which is beneficial for the development of beam catenary action under large displacements due to a column removal. The geometries of the connections modelled in the parametric study are shown in Fig. 5; these were adopted from the Steel Construction Institute (SCI) *Joints in Steel Construction: Simple Connections to EC3* [47] to represent real steel frame beam-to-column connection configurations likely to be used in practice.

The beams and columns were carbon steel S355 UB406 \times 178 \times 74 and UC305 \times 305 \times 137, respectively for both the WA and TSWAC connections. Two angle cleat sections, L150 \times 90 \times 8 and L150 \times 90 \times 12, were employed for each connection to investigate the effect of angle thickness on the overall connection behaviour. The widely used EN 1.4301 austenitic stainless steel was selected for the angle cleats in all the connection models, except for the reference carbon steel connection models, where S275 angles were used for comparison. M20 bolts were adopted in all connection models. Four types of bolt materials were considered, which included austenitic A4-80 fully threaded, austenitic A4-80 partially threaded, duplex DX109 fully threaded and carbon steel 8.8 fully threaded bolts. For the austenitic A4-80 stainless steel bolts, both fully threaded and partially threaded bolts were considered as the strength and ductility of the shank and thread parts are known to be significantly different [48,49], and the impact of that on the connection response needs to be investigated. All bolts were modelled as snugtightened. It was concluded that the stainless steel bolt-preload significantly affect the initial stiffness but has no significant effect on the observed failure mode, ultimate load resistance and deformation

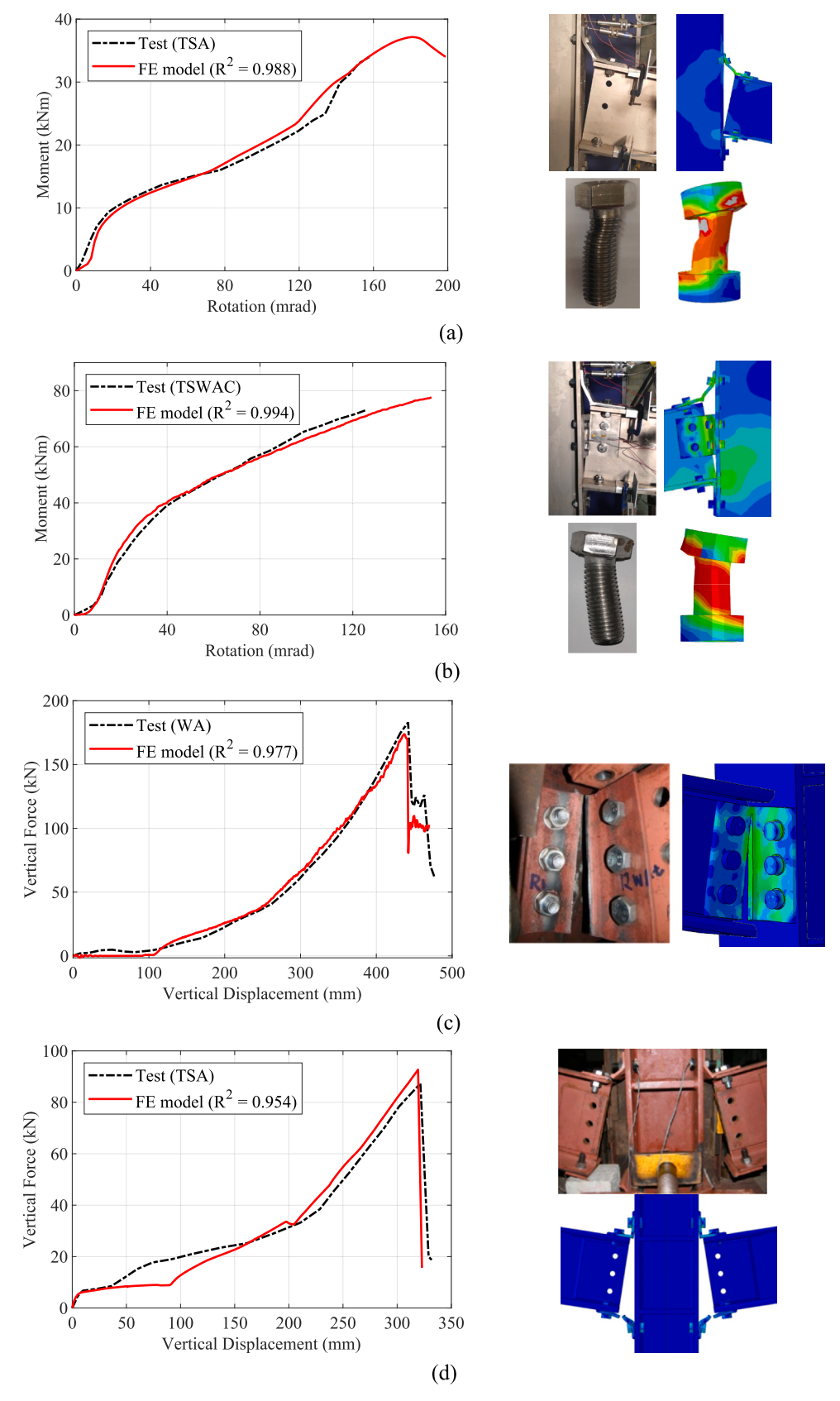


Fig. 2. Comparison of test and FE results for (a) TSAC connection in [31]-(b) TSWAC connection in [31] stainless steel bolted connection and (c) WA connection – specimen WA-8 in [20]-(d) TSAC connection – specimen TS-8 in [20] carbon steel two-sided bolted beam-to-column connection tests.

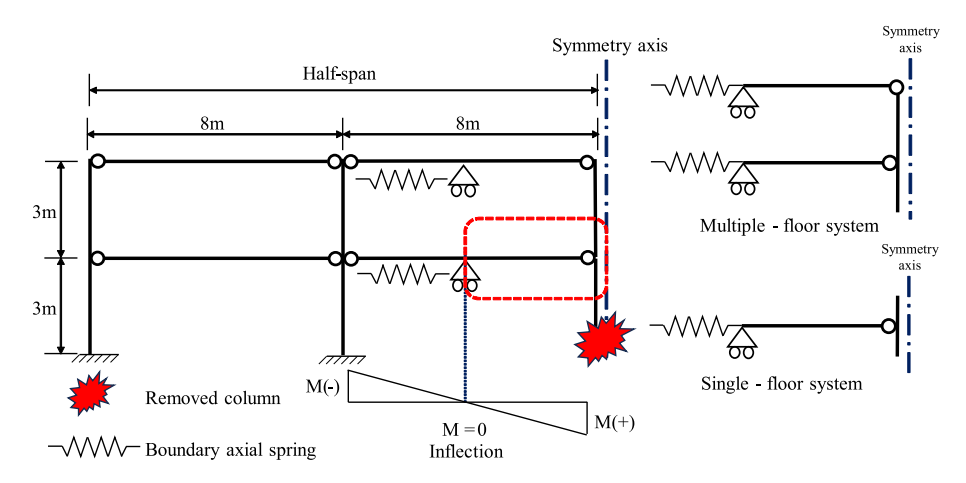


Fig. 3. Idealization of the structural frame for the assessment of column removal models.

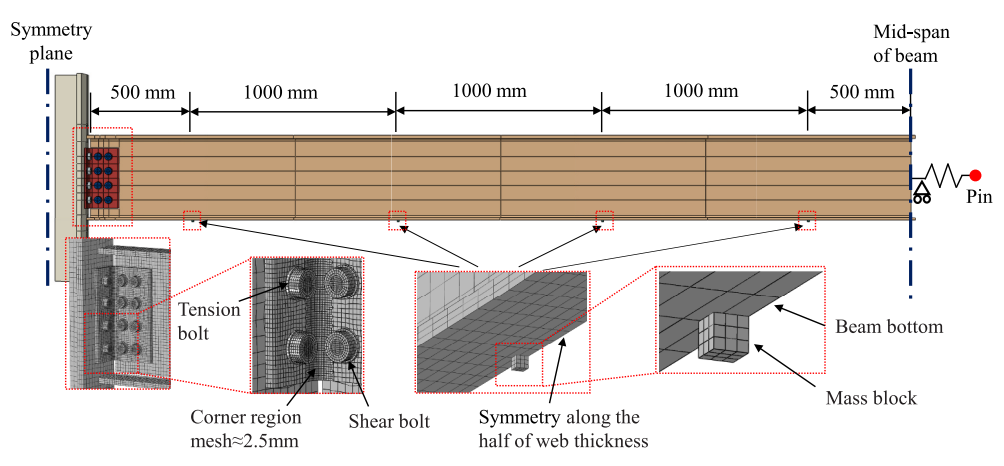


Fig. 4. Schematic representation of the parametric study beam-to-column connection models.

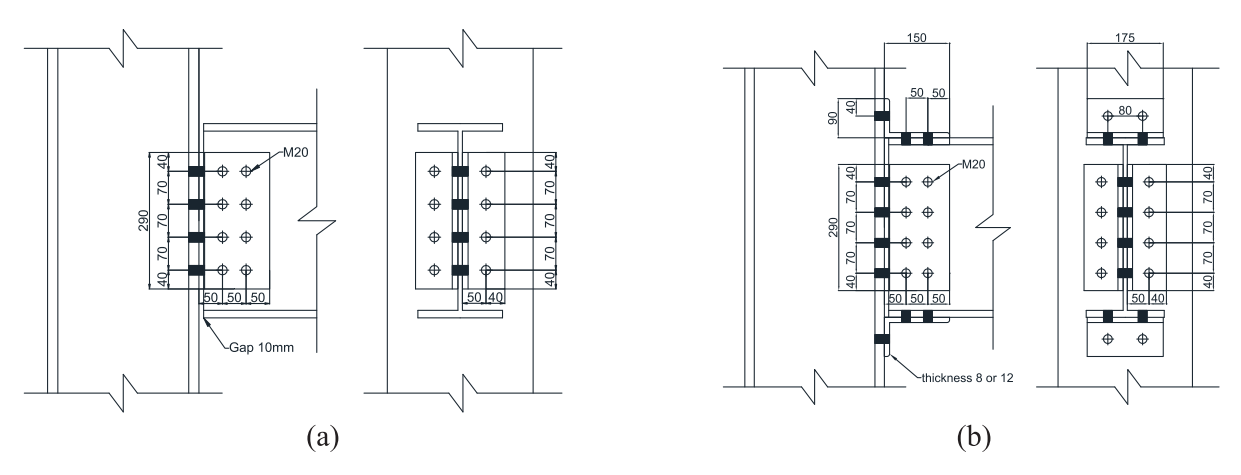


Fig. 5. Joint details of the parametric study specimens. (a) WA parametric model connection and (b) TSWAC parametric model connection.

capacity [50,51]. Since the overall response of the joints and sub-frame systems is governed by plastic material deformation, not including bolt preload is not expected to have any significant effect on the obtained results and the validity of our conclusions.

3.3. Material modelling for parametric study

For the parametric study, the full range stress-strain response of the connection components, including the bolts and angle cleats, which

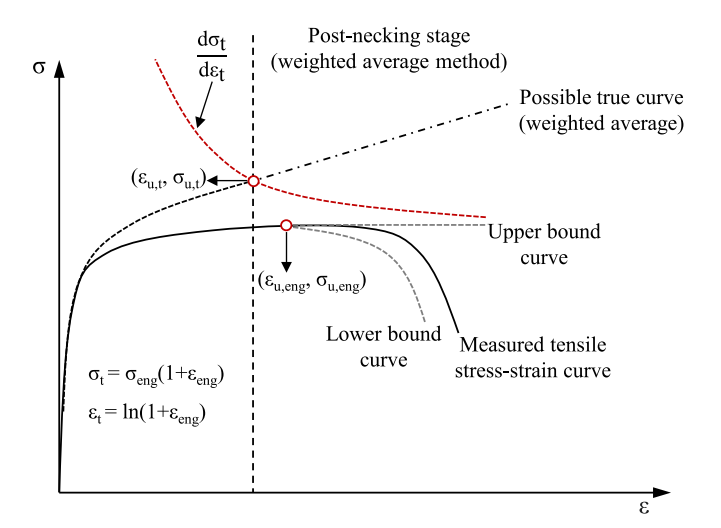
could cause fracture needs to be accurately defined in the models. To this end, stress-strain relationships covering the pre-necking, postnecking and fracture of these components were first developed, as described hereafter. For the bolts, the measured tensile and shear stress-strain or force-displacement responses were taken from literature. For A4–80 fully threaded M20 bolts, A4–80 partially threaded M20 bolts and 8.8 fully threaded M20 bolts, data reported in [33] were adopted, while for DX109 fully threaded M20 bolts, data reported in [32] were used. For the EN 1.4301 and S275 angle cleats, tensile stress-strain data

from [35,38], respectively were used. The pre-necking stress-strain responses were directly taken from the measured engineering stress $\sigma_{\rm eng}$ and strain $\varepsilon_{\rm eng}$ data and input into ABAQUS in the form of true stress $\sigma_{\rm t}$ and true strain $\varepsilon_{\rm t}$ as defined by the relationships given by Eqs. (1) and (2), respectively. To represent the post-necking stress-strain response, a 'weighted average' approach, was adopted where it is assumed that the true stress-strain curve of the material after necking lies between an upper and a lower bound as shown in Fig. 6. The actual true stress-strain curve is determined through an iterative trial-and-error approach by adjusting a weighted averaging factor w between these upper and lower limits until an acceptable agreement is reached between the test and the FE analysis results.

For the choice of the upper and lower bounds, a similar approach to that initially proposed by Ling [52] and more recently adopted by Song et al., [33] was adopted. The upper bound of the post-necking true stress-strain was taken as the one corresponding to the perfect plastic extension of the pre-necking engineering stress. Eqs. (3) and (4) present the assumed upper bound responses in terms of engineering ($\varepsilon_{\rm eng}$, $\sigma_{\rm eng}$) and true (ε_t , σ_t) stress-strain curves, respectively, where $\sigma_{u,eng}$ and $\varepsilon_{u,eng}$ are the engineering stress and strain and $\sigma_{u,t}$ and $\varepsilon_{u,t}$ are the true stress and strain at the ultimate point, respectively. A power-law relationship was used to estimate the lower bound true stress-strain response as given by Eq. (5). This assumption takes into account the reduction in the crosssectional area due to necking. Therefore, after introducing the weighted average parameter w, the complete post-necking true stress-strain relationship may be estimated as given by Eq. (6). The weighted average parameter w can be taken as a constant for all strain values or in some cases varying w with strain has been reported to provide better results. Song et al., [33] adopted a variable w, as defined by Eq. (7), where a_1 and a_2 are constants. The calibration of w (or a_1 and a_2) is an iterative process that involves starting with an initial value for w (or a_1 and a_2) and obtaining the corresponding true stress-strain. The FE analysis is then carried out with this assumed post-necking response and the numerically obtained load-displacement response is compared with the experimental one. This is repeated until a good match between the test post-necking stress-strain curve and the FE simulation is obtained. The weighted average method with varying w parameter was adopted in this study to model the post-necking stress-strain response of the connection components prior to fracture.

$$\sigma_t = \sigma_{eng} \big(1 + \epsilon_{eng} \big) \ \, \text{for} \, \epsilon \leq \epsilon_{u,eng} \tag{1} \label{eq:tau_eng}$$

$$\varepsilon_t = ln(1 + \varepsilon_{eng}) \quad \text{for } \varepsilon \le \varepsilon_{u,t}$$
(2)



 $\begin{tabular}{ll} {\bf Fig.} & {\bf 6.} {\bf \ Schematic \ \ representation \ \ of \ \ pre- \ \ and \ \ post-necking \ \ stress-strain \ response modelling. \end{tabular}$

$$\sigma_{eng} = \sigma_{u,eng} \quad \text{for } \epsilon > \epsilon_{u,eng}$$
 (3)

$$\sigma_t = \sigma_{u,t}.exp(\epsilon_t - \epsilon_{u,t}) \quad \text{for } \epsilon > \epsilon_{u,t} \tag{4}$$

$$\sigma_{t} = \sigma_{u,t} (\varepsilon_{t}/\varepsilon_{u,t})^{\varepsilon_{u,t}} \quad \text{for } \varepsilon > \varepsilon_{u,t}$$
 (5)

$$\sigma_t = \sigma_{u,t} \big[w \cdot exp \big(\epsilon_t - \epsilon_{u,t} \big) + (1+w) \big(\epsilon_t \big/ \epsilon_{u,t} \big)^{\epsilon_{u,t}} \, \big] \quad \text{for } \epsilon > \epsilon_{u,t} \tag{6} \label{eq:delta_t}$$

$$w = 1/[1 + a_1(\varepsilon_u - \varepsilon_{u,t})^{a_2}] \quad \text{for } \varepsilon_t > \varepsilon_{u,t}$$
 (7)

Two fracture models, namely the void growth model (VGM) [39-41] and the Bao-Wierzbicki model (B-W) model [53,54] were employed for the simulation of the fracture of the angle cleats and the bolts, respectively. Schematic representations of both fracture models are shown in Fig. 7. The simplified B-W model was adopted for the fracture simulation of the bolts as they experience a combination of tensile and shear stresses. The model provides an explicit equation relating the plastic fracture strain $\varepsilon_{pl,f}$ to the stress triaxiality η over the full stress triaxiality range, covering combined shear and compression, combined shear and tension and tensile failures, as presented by Eq. (8-11). In this model, η_0 is the stress triaxiality under pure tension i.e., $\eta_0 = 1/3$ and C_1 and C_2 are fracture parameters. Fig. 7 illustrates the relationship between plastic fracture strain $\varepsilon_{pl,f}$ and stress triaxiality $\eta.$ The model fracture parameters C_1 and C_2 are plastic fracture strains at pure tension ($\eta = 1//$ 3) and pure shear ($\eta = 0$), respectively. The VGM model was adopted for the fracture simulation of the angle cleats, which are subjected to tension-dominant ductile fracture. The relationships between the plastic fracture strain $\varepsilon_{pl,f}$ and stress triaxiality η as adopted by the VGM model is presented in Eq. (12), where $C_{\rm VGM}$ is a material dependent parameter.

$$\varepsilon_{\text{pl,f}} = \infty \quad \text{for } \eta = -1/3 \text{ (no failure)}$$
 (8)

$$\varepsilon_{pl,f} = \frac{C_1}{(1+3\eta)} \text{ for } -1/3 < \eta \le 0 \text{ (combined compression\&shear)}$$
(9)

$$\varepsilon_{\text{pl,f}} = C_1 + (C_2 - C_1) \left(\frac{\eta}{\eta_0}\right)^2$$
 (10)

for $0 < \eta \le \eta_0$ (combined tension&shear)

$$\epsilon_{pl,f} = \frac{C_2 \eta_0}{\eta} \quad \text{for } \eta > \eta_0 (\text{tension failure}) \eqno(11)$$

$$\epsilon_{pl,f} = C_{VGM} e^{(-1.5\eta)} \quad \text{for } \eta > \eta_0 (\text{tension failure}) \eqno(12)$$

The fracture parameters can be calibrated by iteratively simulating a

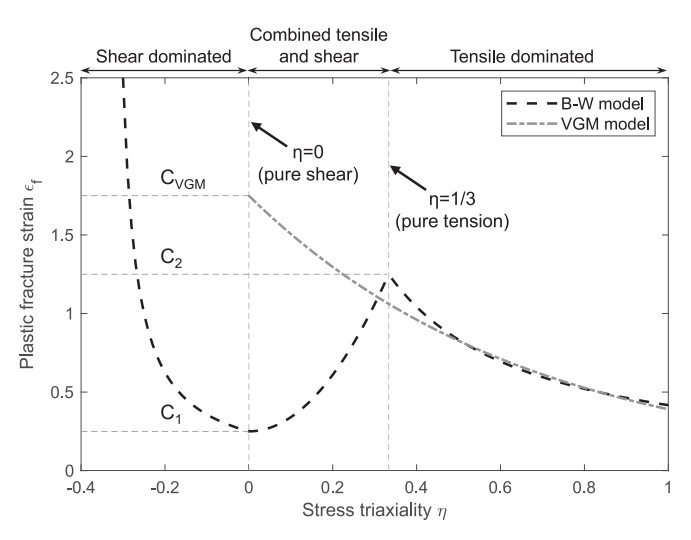


Fig. 7. Fracture strain versus triaxiality relationships.

coupon model of the test material considered and updating its postnecking response parameters until a good agreement between the experimental and numerical response is obtained. Since the C_1 and C_2 relate to tensile and shear failure, respectively, test results from a pure tensile test and a pure shear test on a bolt specimen are utilised to calibrate these parameters, whereas for the C_{VGM} only the pure tensile response is required. Finite element fracture simulation of highly ductile metals poses a significant challenge, particularly in controlling element behaviour under the post-necking stage, and researchers have explored small mesh sizes and different element types with increased integration points to try to improve the results. However, these approaches may require extensive computational resources and time, which is not efficient when the calibrated fracture model is to be used for large scale models like the ones developed herein. Therefore, this study aims to strike a balance between accuracy and computational efficiency and thus employs element sizes larger than the ones normally considered for material coupon modelling.

To ensure consistent fracture performance in the beam-to-column connection models, the same mesh size and topology as the material calibration models were employed. A global mesh size of 2.5 mm was employed for all fracture calibration models, with the exception of the smooth section of the very ductile A4–80 partially threaded bolt, where a refined mesh size of 1.5 mm was employed. This refinement helps to more accurately simulate possible failures, as this is the potential shear failure plane, in both material calibration and parametric study models. To calibrate the post-ultimate stress-strain response and fracture of the bolts, two models, a tensile model and a shear model, were created for each bolt, key features of which are presented in Fig. 9. The post-necking and fracture calibration process adopted is described schematically in Fig. 10. The calibrated material properties including the weighted average post-necking stress-strain response parameters a_1 and a_2 , and the fracture parameters C_1 and C_2 and the C_{VGM} for each of the connection components are reported in Table 2. Comparisons between the experimental and numerically obtained load-displacement responses for all bolt grades under shear and tension, are depicted in Fig. 8, where the experimental curves are the ones reported by Song et al. [33].

4. Results, analysis and discussions

4.1. Cantilever models

The cantilever model was employed to evaluate the moment-rotation behaviour of the WA and TSWAC connections, focusing on key connection response parameters such as initial rotational stiffness $S_{\rm j,ini}$, plastic moment resistance $M_{\rm j,R}$, ultimate moment resistance $M_{\rm j,max}$ and corresponding rotation at ultimate resistance $\Phi_{\rm j,u}$, as shown schematically in Fig. 11. Fig. 12 (a) and (b) depict the moment-rotation curves for these connections, where the boundaries for pinned and rigid connections, as defined by EN 1993-1-8 [55], are also illustrated. This

visualisation reveals that the simulated WA connections align with the characteristics of a typical pinned connection, while the TSWAC connections fall within the semi-rigid category. The model labelling system adopted is defined as follows: 't8' and 't12' represent 8 mm or 12 mm angle thicknesses, respectively; '8.8', 'A4-80' and 'DX109' represent the bolt material grade, and 'FT' and 'PT' represent fully threaded and partially threaded bolts, respectively. A summary of the connection response parameters $S_{i,ini}$, $M_{i,R}$, $M_{i,max}$, and $\Phi_{i,u}$, extracted from the moment-rotation curves of the WA and TSWAC models, is presented in Tables 3 and 4, respectively. The initial rotational stiffness $S_{i,ini}$ was based on the secant stiffness corresponding to a point on the momentrotation response, where the secant stiffness at that point deviated by more than 20 % from the average of the secant stiffness values of the preceding data points, as describe [56]. The initial nonlinear region of the moment-rotation response, associated with the initial slip of nonpreloaded bolts, was excluded from the secant stiffness evaluations. The equal-area method, as shown in Fig. 11, was used to estimate the post-yield stiffness, where the two areas enclosed by the hardening slope and the response data, between the identified so called yield moment $M_{\rm v}$ and the ultimate moment $M_{j,max}$, are equal. The plastic moment resistance $M_{i,R}$ was then determined as the intersection between the initial rotational stiffness and the post-vield stiffness.

As shown in Fig. 12 (a), the stiffness of the WA connections exhibits a sudden increase at around 70 mrad rotation, caused by the contact between the beam's lower flange and the column flange, which effectively increases the lever arm and enhances the connection stiffness. The TSWAC connections exhibits considerably higher stiffness compared to the WA connections, primarily due to the presence of the top and seat angle cleats, which provided a direct connection between the beam flanges and the column thus facilitating moment transfer and enhancing the overall connection rotational stiffness. Failure in the WA connections typically involves fracture of the column flange bolts in tension, progressing from the top bolt row downwards. Similarly, failure in TSWAC connections began with tension fracture of the top angle column flange bolts, followed by fracture of the upper bolts in the web angle. The type and material of bolts significantly influences both moment capacity and ductility. Compared to carbon steel connections, the WA stainless steel connections using A4–80 bolts showed approximately 25 % to 72 % higher ultimate moment capacities, while those with DX109 bolts exhibited increases of around 64 % to 70 %. Similarly, for the TSWAC connections, stainless steel models achieved significantly higher maximum moment capacities than carbon steel ones, with A4-80 bolts showing increases of 11 % to 116 % and DX109 bolts showing 61 % to 63 % higher capacities. Stainless steel bolts, known for their higher ductility compared to carbon steel bolts, allowed the connections to sustain larger rotations before failure, enhancing overall structural robustness. This is more pronounced for partially threaded A4-80 bolts, which lead to the highest rotation among all connections considered.

Table 2Material properties and calibrated post-necking and fracture parameters.

Material	E	f_{y}	$f_{ m u}$	ε_{u}	n	n'u	a_1	a_2	C_1	C ₂	$C_{ m VGM}$	Mesh
	(MPa)	(MPa)	(MPa)	(%)							-	(mm)
A4–80 bolt (fully threaded)	191,457	629	835	12.0	10.2	10.7	15.00	1.8	0.45	0.89	-	2.5
A4–80 shank (partially-threaded)	188,129	535	724	36.8	21.3	14.5	0.65	0.5	0.58	2.00	-	1.5
A4–80 thread (partially-threaded)	188,129	775	950	45.4	-	-	-	-	-	-	-	2.5
DX109 bolt (fully threaded)	185,300	833	1050	1.4	2.5	3.7	9.00	1.2	0.65	1.60	-	2.5
G8.8 bolt (fully threaded)	200,000	680	941	6.2	-	-	5.00	1.0	0.44	0.16	-	2.5
EN1.4301 angle cleat S275 angle cleat	197,600 210,000	239 275	657 430	46.2 21.7	12.2	2.5	_	_	_	_	1.8 1.2	2.5 2.5

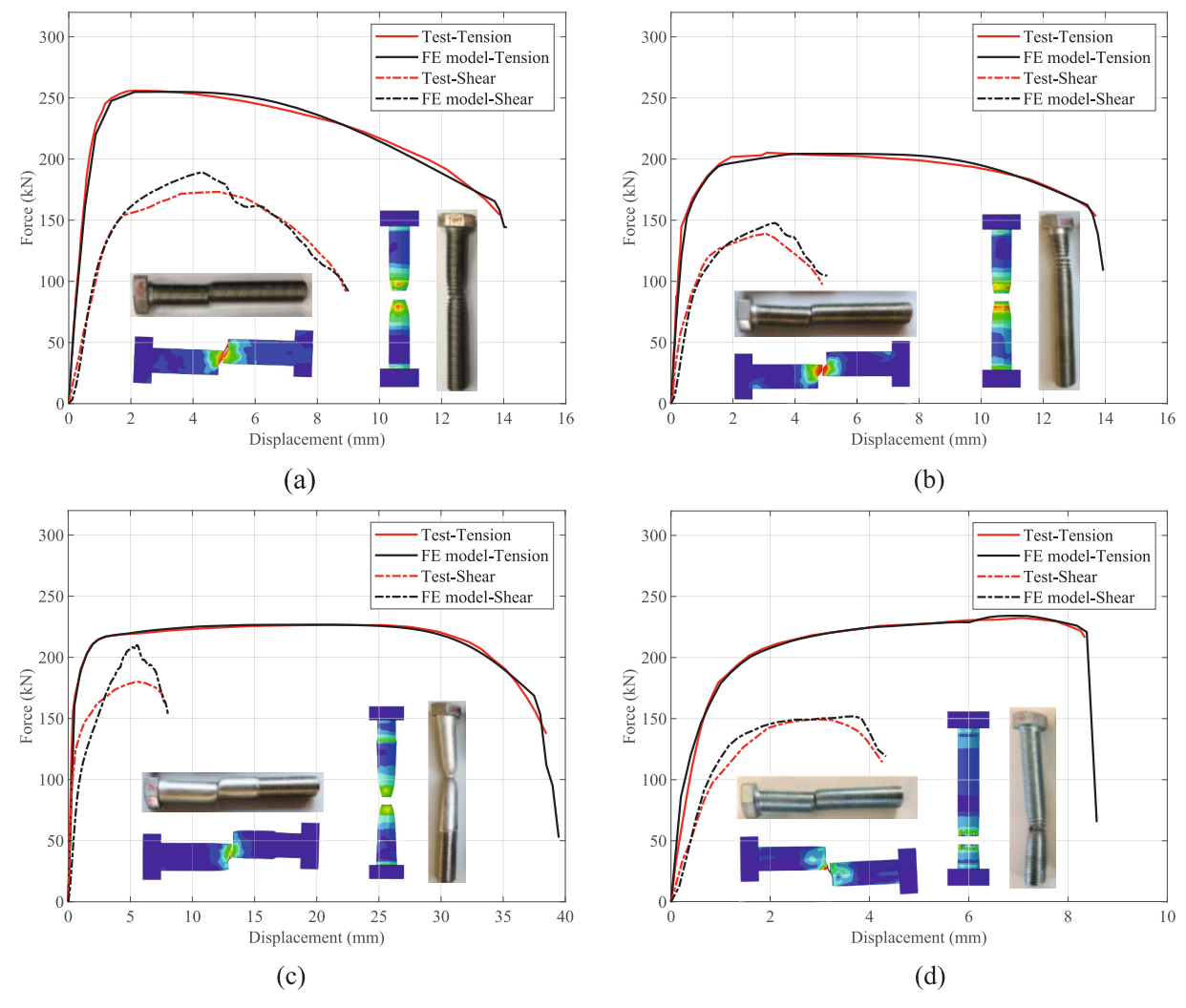


Fig. 8. Comparison of bolt test and FE calibrated tensile and shear force-displacement responses. (a) DX109 fully-threaded bolt, (b) A4-80 fully-threaded, (c) A4-80 partially-threaded bolt and (d) 8.8 fully-threaded bolt.

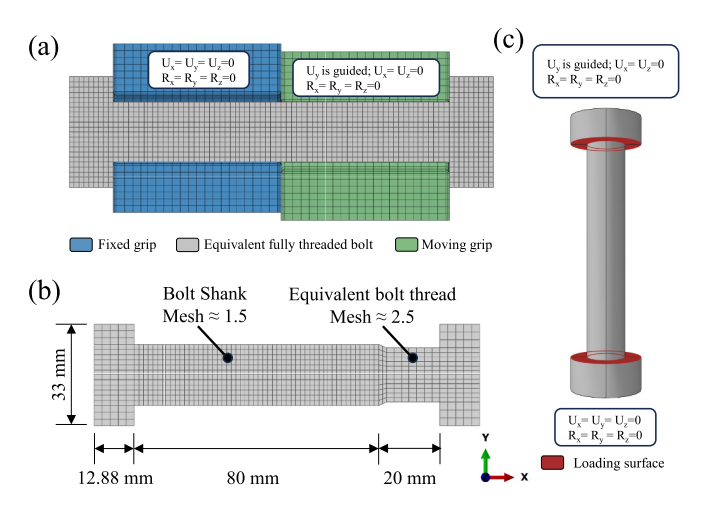


Fig. 9. FE model and mesh diagram for fully and partially threaded bolts in tension and shear: (a) Loading and boundary conditions for bolts under shear; (b) Sectional view of partially threaded bolt mesh; (c) Loading and boundary conditions for bolts under tension.

4.2. Static column removal models

Figure 13 shows the results of the static column removal analyses for the WA and TSWAC connections. For each connection type, the changes in the column vertical force and the beam horizontal reaction force with vertical displacement at the beam-to-column connection is plotted. A summary of the maximum vertical $F_{v,max}$ and horizontal $F_{h,max}$ forces for the fully restrained (FR) and partially restrained (PR) models is presented in Table 5. The WA and TSWAC connections under column removal conditions exhibited three stages of behaviour, namely flexuredominated, transition and catenary action dominated - representing the shift in the load-bearing mechanisms from flexure to catenary action with increasing deformation. At small vertical displacements, both WA and TSWAC connections primarily resist loads through flexural action, exhibiting high initial stiffness and a linear increase in vertical load. However, the WA connection quickly transitioned to the catenary phase, while the TSWAC connection experienced a prolonged flexuraldominated and transition stage, before reaching catenary action, benefiting from the top and seat angle cleats that enhance flexural resistance and initial stiffness. Despite these differences, the maximum vertical load capacity for both connections was comparable. This result contrasts with the cantilever model, suggesting that upon column removal, the nominally weaker WA connection can, in fact, achieve a higher load capacity by more effectively utilizing catenary action

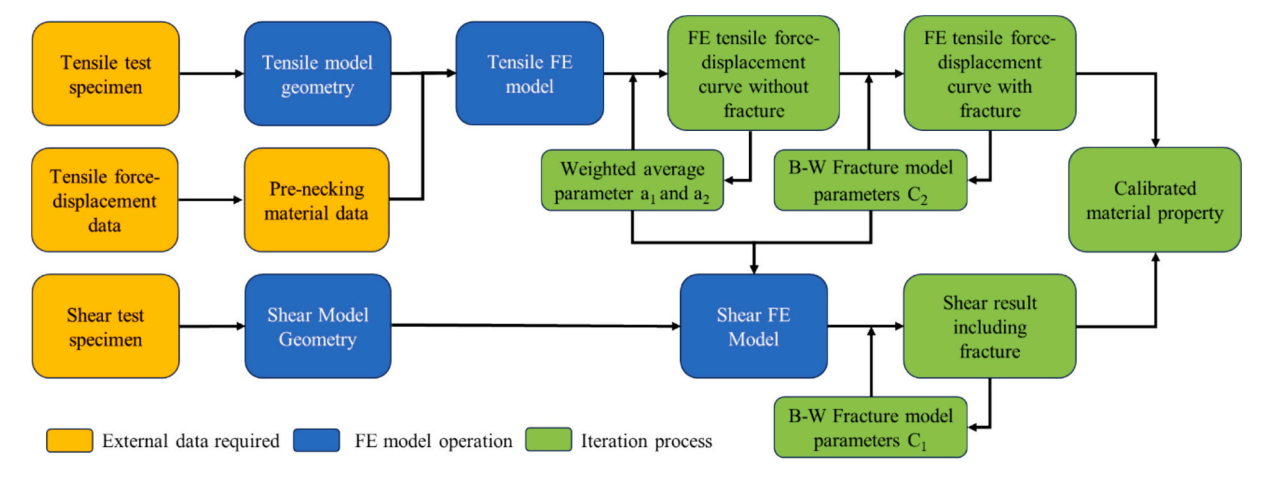


Fig. 10. Flowchart of material model calibration process.

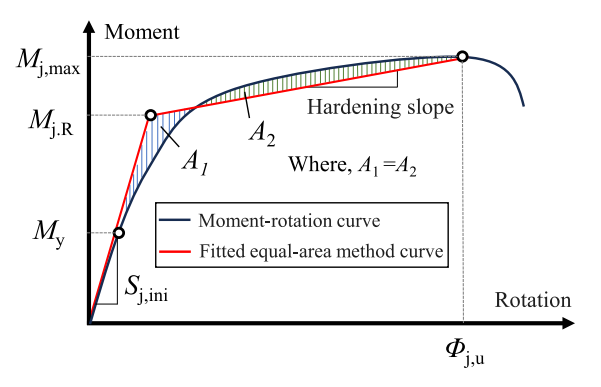


Fig. 11. Equal-area method for deriving moment-rotation parameters.

through their higher ductility. All parametric connection models failed by bolt fracture, except t8-A4-80-PT, which exhibited plate bearing around the bolt hole.

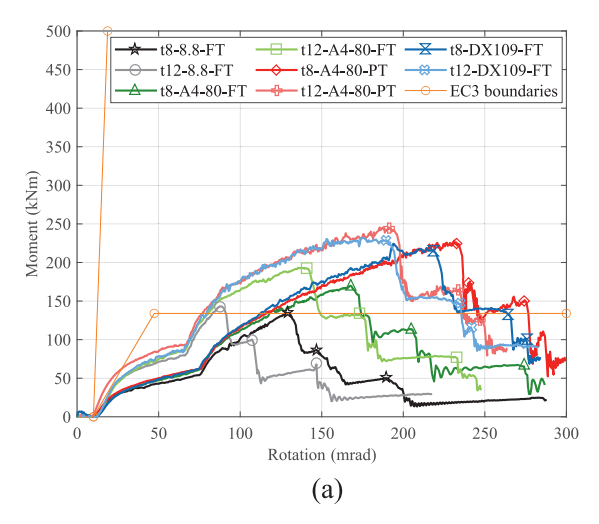
4.2.1. Effect of angle cleat thickness

The performance of WA and TSWAC connections is influenced by the thickness of the angle cleat, which affects both the initial stiffness and deformation capacity. While 12 mm angle cleats exhibited increased connection stiffness, the thinner 8 mm cleats demonstrated enhanced vertical load and rotational capacities, as they allowed more

deformations to take place, which enhanced the extent of catenary action development and delayed final failure by bolt fracture. Fig. 14 shows the typical deformation behaviour of the 8 m and 12 mm angle cleat before failure. The 8 mm angle cleat exhibited a well-developed yield line at the corner and distributed strain along its full length prior to bolt fracture, indicating superior ductility. In contrast, the 12 mm angle cleat exhibited lower strain levels and more limited plastic deformation. These findings highlight a trade-off between stiffness and rotational capacity, suggesting that the optimal cleat thickness should be selected to maximise energy absorption under large deformations and avoid brittle failure. In this context, thinner angle cleats may offer improved overall structural resilience.

4.2.2. Effect of bolt material

The behaviour of WA and TSWAC connections under a column removal scenario was influenced by the chosen bolt material, which included carbon steel (G8.8), austenitic stainless steel (A4–80, fully and partially threaded), and duplex stainless steel (DX109). Bolt material notably affected both vertical load capacity and rotational behaviour. Both WA and TSWAC connections with carbon steel bolts (G8.8) exhibited the lowest load carrying capacity compared to those with stainless steel bolts. In contrast, WA and TSWAC connections with A4–80 fully threaded bolts demonstrated a 50 %–100 % increase in vertical load carrying capacity compared to the same connections with fully threaded G8.8 bolts. This significant improvement in capacity is primarily attributed to the higher ductility and tensile strength of



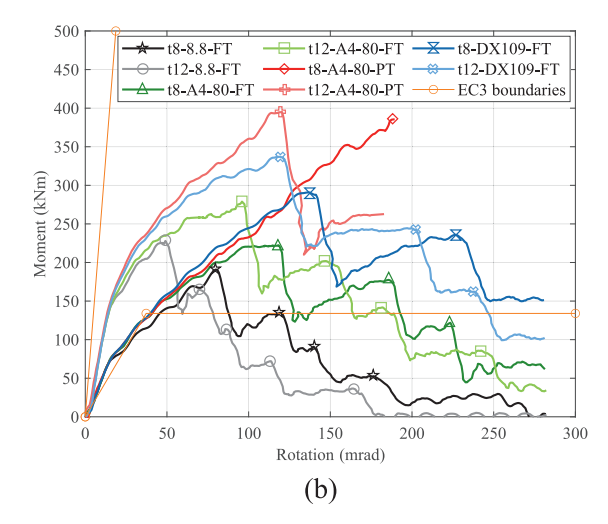


Fig. 12. Moment-rotation curves of WA and TSWAC cantilever models. (a) WA - cantilever moment-rotation and (b) TSWAC - cantilever moment-rotation.

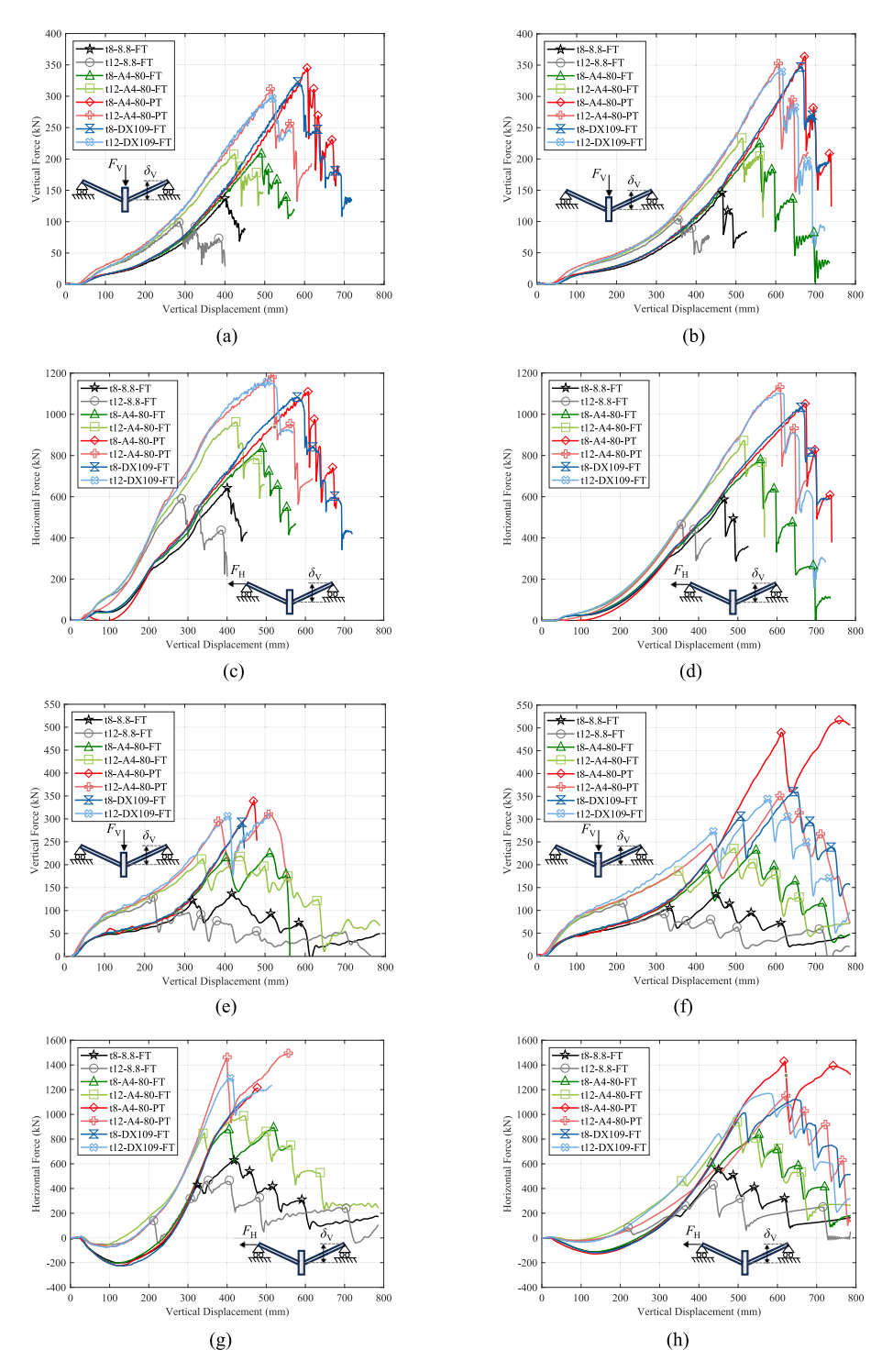


Fig. 13. Vertical and horizontal force-displacement responses of static column removal models. (a) WA vertical force, fully restrained (FR), (b) WA vertical force, partially restrained (PR), (c) WA horizontal force, fully restrained (FR), (d) WA horizontal force, partially restrained (PR), (e) TSWAC vertical force, fully restrained (FR), (f) TSWAC vertical force, partially restrained (PR), (g) TSWAC horizontal force, fully restrained (FR) and (h) TSWAC horizontal force, partially restrained (PR).

stainless steel bolts, which allow for greater deformation and facilitate the development of catenary action, enhancing the overall load-bearing performance.

Among the A4–80 bolts, partially threaded bolts outperformed fully threaded ones by exhibiting higher rotational and vertical load capacities in both WA and TSWAC connections, attributed to the enhanced ductility of the shank material in partially threaded bolts. Fig. 15 (a) illustrates the contribution of the catenary mechanism to the vertical load-bearing capacity of the fully threaded and partially threaded t12-

A4–80 specimens, derived from the vertical component of the beam internal force. Under large displacements, where catenary action becomes the dominant contributor to vertical resistance, the ductility of the connection becomes a critical factor in determining vertical capacity. For the A4–80 specimens, the enhanced rotational capacity observed in the partially threaded bolts is primarily attributed to the increased ductility of the bolts. This is supported by the equivalent plastic strain distribution in the angle cleats, shown in Fig. 15 (b) and (c), which show analogous deformation patterns in both the A4–80-PT and A4–80-FT

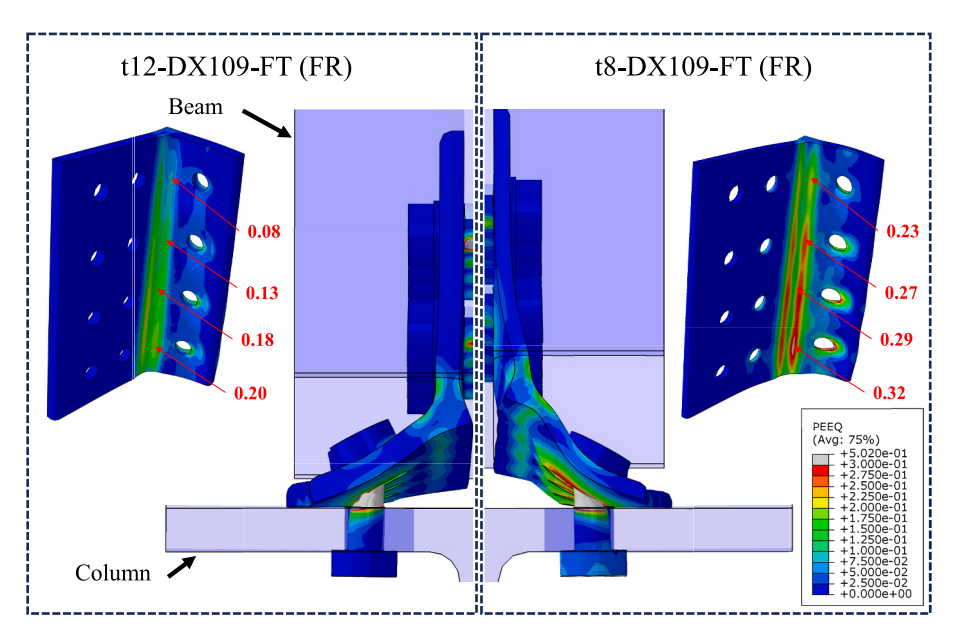


Fig. 14. Equivalent plastic strains for WA-DX109-FT (FR) with 8 mm and 12 mm thick angle cleats.

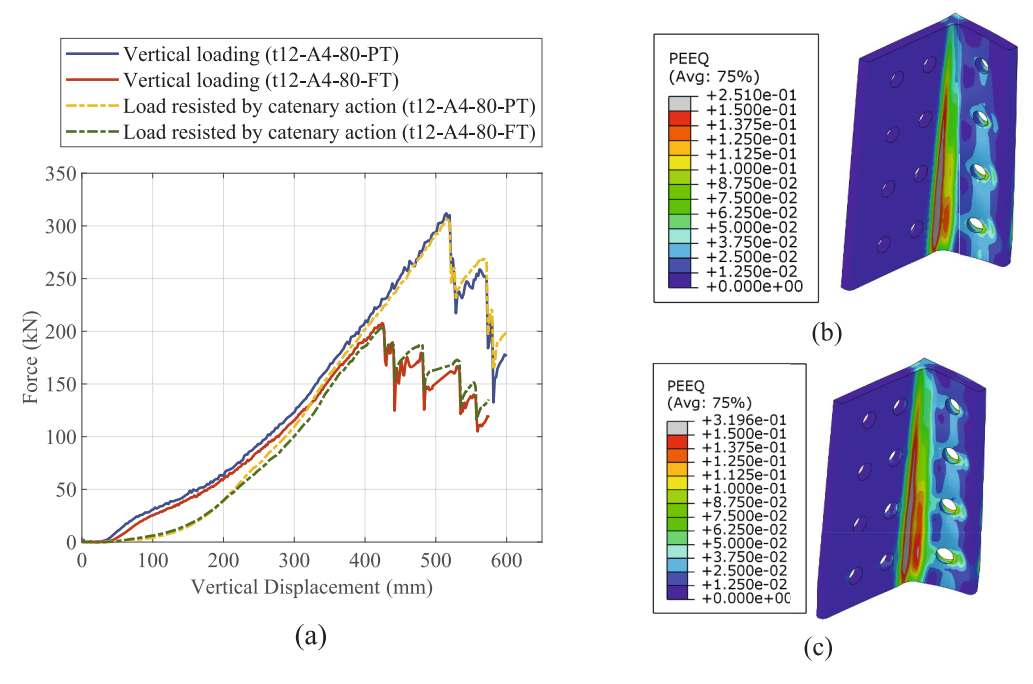


Fig. 15. Development of catenary action and evolution of angle equivalent plastic strains for t12-A4-80 (FR). (a) Vertical force and contribution of catenary action curve of specimen WA-t12-A4-80 (RF), (b) Angle yield line in WA-t12-A4-80-FT (FR) and (c) Angle yield line in WA-t12-A4-80-PT (FR).

configurations before failure. Compared to austenitic stainless steel, duplex bolts offered higher strength, enabling the connection to withstand greater loads while maintaining ductility, leading to improved load capacity and more pronounced catenary action through greater deformation of the steel angle. In summary, bolt material significantly influences load capacity and rotational behaviour in angle connections. Duplex stainless steel bolts (DX109) and partially threaded austenitic stainless steel bolts (A4–80) offer the highest load capacity due to very high strength and very high ductility respectively. Carbon steel bolts (G8.8), while suitable for lower load requirements, exhibit lower ductility and overall performance compared to their stainless steel counterparts.

4.2.3. Effect of beam end restraints

Boundary conditions for WA and TSWAC connections under column removal scenarios are crucial in determining their ultimate performance. Two types of boundary conditions, partially restrained (PR) and fully restrained (FR) at the beam ends, were investigated for each connection type. The partial restraint condition accounts for interaction with the surrounding frames, while the full restraint condition assumes rigid boundaries. Although full restraint is uncommon in real structures, as even stiff surrounding frames exhibit some flexibility, it represents scenarios where column loss occurs near high-stiffness structures, such as low floors or areas adjacent to shear walls. In all cases, full restraint enhanced the initial stiffness of the connections. In the flexure-dominated stage of TSWAC, even minor boundary deformation significantly affected arching action, thus impacting early stiffness. The

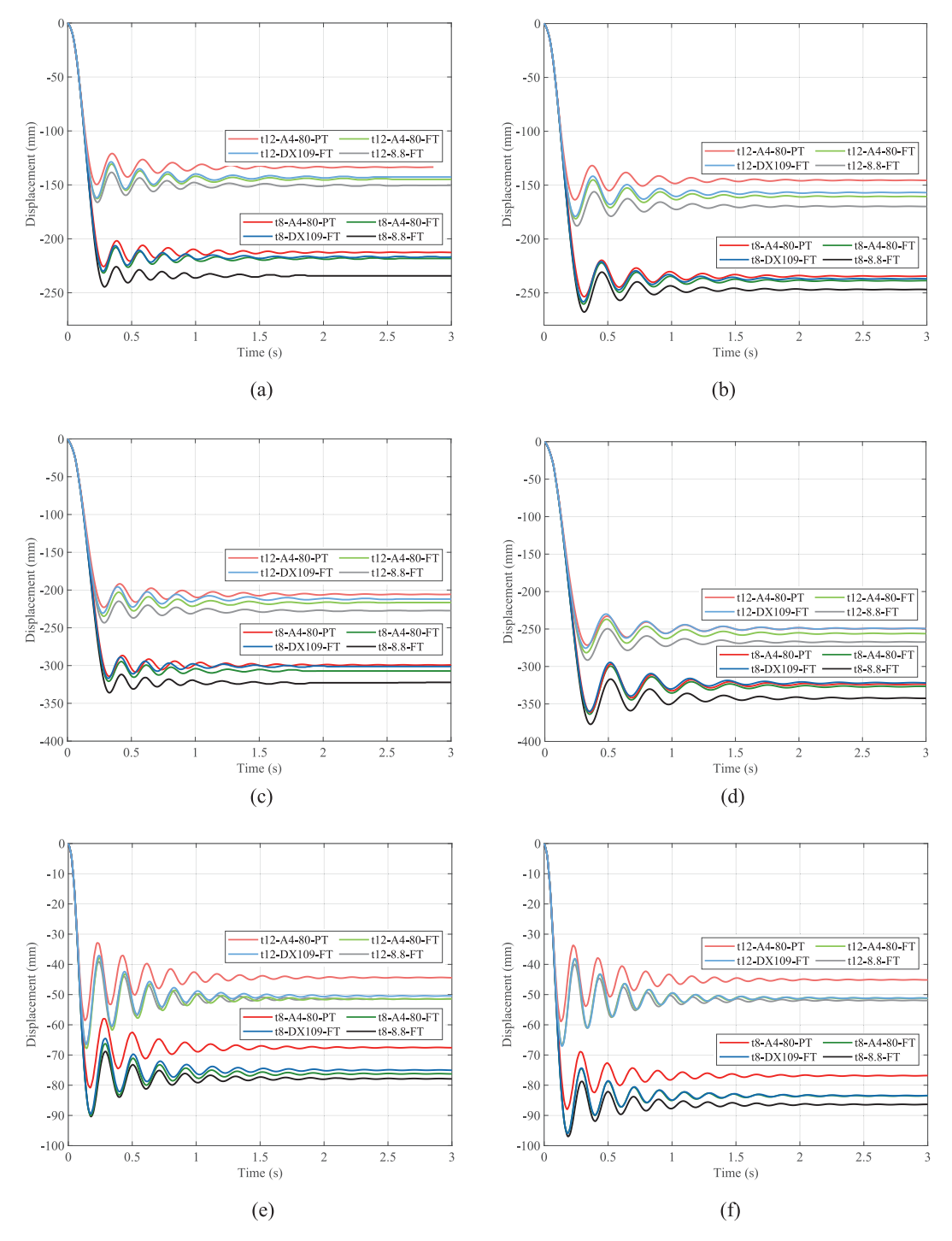


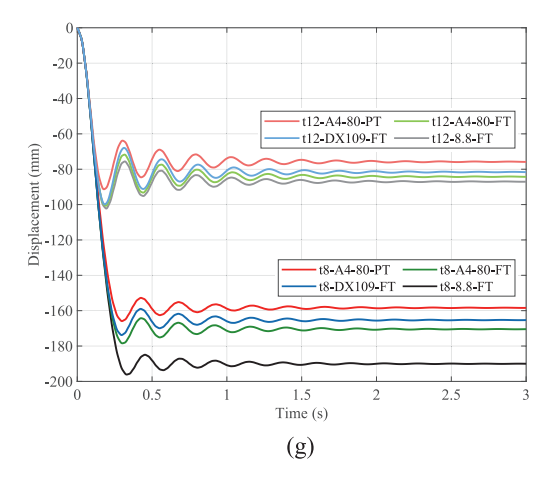
Fig. 16. Time-displacement curves for dynamic column removal. (a) WA fully restrained 10 kN/m UDL, (b) WA partially restrained 10 kN/m UDL, (c) WA fully restrained 20 kN/m UDL, (d) WA partially restrained 20 kN/m UDL, (e) TSWAC fully restrained 10 kN/m UDL, (f) TSWAC partially restraint 10 kN/m UDL, (g) TSWAC fully restrained 20 kN/m UDL and (h) TSWAC partially restrained 20 kN/m UDL.

partially restrained connections exhibited higher vertical displacement, which benefits catenary action essential for resisting vertical loads. This effect is particularly pronounced in stronger connections with thicker angles; for example, in the WA connection with 12 mm angle steel, the maximum vertical loading capacity increased by about 10 %. Although boundary conditions influence the load capacity and rotational behaviour of WA and TSWAC connections, the level of restraint provided by the surrounding frame is typically fixed and cannot be altered during design. Therefore, this parameter is more often considered during the

evaluation phase to identify vulnerable locations within the frame structure.

4.3. Dynamic column removal models

In this section, sudden column removal was used to assess the dynamic response of WA and TSWAC connections, simulating a worst case scenario in a real-world progressive collapse situation. In most cases, the column loss will be more gradual than the instantaneous one assumed



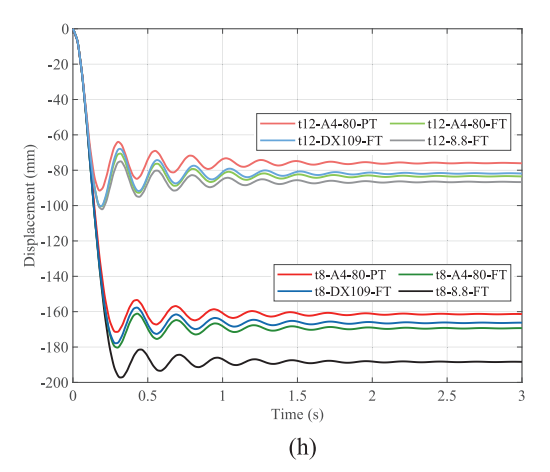


Fig. 16. (continued).

 Table 3

 Summary of FE moment-rotation response parameters for WA cantilever models.

Model	S _{j,ini} (kNm/rad)	M _{j.R} (kNm)	M _{j,max} (kNm)	$\Phi_{ m j,u}$ (mrad)
t8-8.8-FT	2838	24.8	136.1	127.7
t12-8.8-FT	4279	48.6	143.1	87.6
t8-A4-80-FT	2644	26.6	169.8	167.7
t12-A4-80-FT	4074	50.6	193.2	135.5
t8-A4-80-PT	2651	31.3	228.3	231.2
t12-A4-80-PT	4407	53.7	245.7	187.7
t8-DX109-FT	2551	26.4	224.2	193.8
t12-DX109-FT	4205	47.6	231.9	195.6

Table 4Summary of FE moment-rotation response parameters for TSWAC cantilever models.

Model	S _{j,ini} (kNm/rad)	M _{j.R} (kNm)	M _{j,max} (kNm)	$\Phi_{ m j,u}$ (mrad)
t8-8.8-FT	4756	69.6	173.5	75.1
t12-8.8-FT	10,584	132.5	201.9	42.3
t8-A4-80-FT	4378	121.3	193.2	109.8
t12-A4-80-FT	12,492	179.9	266.7	91.6
t8-A4-80-PT	6012	77.6	374.4	184.9
t12-A4-80-PT	10,408	185.5	372.6	119.4
t8-DX109-FT	5438	118.3	282.4	133.5
t12-DX109-FT	11,355	214.0	324.1	115.7

herein. The analysis focused on two key variables, the magnitude of the uniformly distributed load (UDL) on the beams and the boundary conditions (partially and fully restrained) at the beam ends. The effect of these parameters was systematically investigated to quantify their influence on the transient time-displacement history following column removal, which are shown in Fig. 16. A summary of the observed maximum displacement $D_{\rm max}$ for the fully restrained (FR) and partially restrained (PR) models is presented in Table 6.

4.3.1. Influence of UDL magnitude and beam end restraint

The magnitude of the UDL impacted the time-displacement behaviour of both WA and TSWAC connections. Higher UDL resulted in larger peak displacements due to the demand for increased load redistribution. For example, doubling the UDL in the WA connection led to a 30 % to 40 % increase in the peak displacement within the first few seconds after column removal. TSWAC connections showed a similar trend, though the top and seat angle cleats provided additional resistance, slightly reducing the displacement increase. Boundary conditions played a critical role in the dynamic response. Full restraints reduced the initial

Table 5Summary of maximum vertical and horizontal forces for static column-removal models.

Model	F _{v,max} ,	F _{v,max} ,	$F_{ m v,max,}$	F _{h,max} ,	F _{h,max} ,	F _{h,max,}
	(kN)	(kN)	$F_{v,max,PR}$	(kN)	(kN)	$F_{ m h,max,PR}$
WA						
t8-8.8-FT	137	145	0.94	641	615	1.04
t12-8.8-FT	101	105	0.96	592	516	1.15
t8-A4-80-FT	209	227	0.92	834	816	1.02
t12-A4–80- FT	208	230	0.91	963	920	1.05
t8-A4-80-PT	345	368	0.94	1110	1090	1.02
t12-A4-80- PT	312	341	0.91	1190	1150	1.03
t8-DX109-FT	322	341	0.94	1080	1060	1.02
t12-DX109- FT	300	329	0.91	1160	1130	1.03
TSWAC						
t8-8.8-FT	143	136	1.05	632	562	1.12
t12-8.8-FT	144	118	1.23	483	441	1.09
t8-A4-80-FT	227	235	0.96	897	837	1.07
t12-A4–80- FT	220	239	0.92	992	945	1.05
t8-A4-80-PT	347	516	0.67	1215	1445	0.84
t12-A4-80- PT	311	356	0.88	1496	1152	1.30
t8-DX109-FT	310	362	0.86	1121	1127	0.99
t12-DX109- FT	314	344	0.91	1307	1170	1.12

displacement and slowed the rate of the displacement increase, offering greater resistance to deformation when the column support was abruptly removed. Conversely, partial restraints allowed more movement, leading to a rapid and pronounced increase in displacements. For instance, the TSWAC connection under partial restraint condition showed a 9 % to 15 % higher peak displacement compared to full restraint condition. This underscores the importance of considering boundary flexibility in dynamic analyses, as it directly influences the structure's ability to absorb and redistribute loads during sudden failures.

4.3.2. Influence of angle thickness and bolt material

Angle cleat thickness affected the dynamic response, particularly the maximum displacement. Thicker angle cleats (12 mm) nearly halved the maximum displacement compared to thinner ones (8 mm), due to the increased stiffness that better resists deformation under dynamic loading. This stiffness not only limited the initial displacement but also improved the load distribution across the connection, reducing the peak

Table 6Summary of maximum displacements for dynamic column-removal models.

Model	$D_{ m max,FR}$ (mm)	$D_{ m max,PR}$ (mm)	$D_{ m max,FR}/$ $D_{ m max,PR}$	$D_{ m max,FR}$ (mm)	D _{max,PR} (mm)	$D_{ m max,FR}/$ $D_{ m max,PR}$
10 kN/m UDL		WA			TSWAC	
t8-8.8-FT	245	268	0.91	90	97	0.93
t12-8.8-FT	166	188	0.88	66	67	0.99
t8-A4-80-FT	232	260	0.89	90	96	0.94
t12-A4-80-FT	163	181	0.9	68	67	1.01
t8-A4-80-PT	226	254	0.89	81	88	0.92
t12-A4-80-PT	150	164	0.91	59	59	0.99
t8-DX109-FT	230	258	0.89	90	96	0.93
t12-DX109-FT	162	179	0.9	67	67	0.99
20 kN/m UDL		WA			TSWAC	
t8-8.8-FT	336	377	0.89	196	197	0.99
t12-8.8-FT	243	291	0.83	102	102	1.00
t8-A4-80-FT	321	364	0.88	178	180	0.99
t12-A4-80-FT	235	282	0.83	101	100	1.00
t8-A4-80-PT	314	361	0.87	166	171	0.97
t12-A4-80-PT	223	272	0.82	91	92	1.00
t8-DX109-FT	317	360	0.88	174	178	0.98
t12-DX109-FT	231	276	0.84	100	100	1.00

displacement. Bolt material also influenced the maximum displacements. Connections using carbon steel bolts exhibited the highest displacement, indicating lower dynamic load resistance. In contrast, connections with DX109 and A4–80 partially threaded bolts showed significantly reduced displacement. The smallest displacement was observed with the A4–80 partially threaded bolts, attributed to their higher ductility and strain-hardening properties, allowing the connection to absorb more energy and resist greater deformations before reaching the maximum displacement.

4.4. Discussion on static and dynamic column removal responses

The dynamic column removal induces inertial effects, damping and structural vibration modes that may lead to amplified or complex structural responses. Therefore, the dynamic increase factor (DIF) is employed to quantitatively characterize these dynamic effects. The DIF is defined as the ratio between peak dynamic response and corresponding static response in equivalent systems, commonly calculated using force or displacement. In this investigation, the DIF is defined as the ratio of the maximum vertical reaction force F_{dy} in the dynamic model at peak displacement and the corresponding static reaction force at identical displacement F_{st} , which are presented in Table 7 and Table 8 for WA and TSWAC fully restrained (FR) and partially restrained (PR) models, respectively. For the WA connections, the DIF ranged from 1.7

Table 7Comparison of static and dynamic column removal results for WA.

Model	F _{dy,FR} (kN)	F _{st,FR} (kN)	$\mathrm{DIF}_{\mathrm{FR}}$	F _{dy,PR} (kN)	F _{st,PR} (kN)	$\mathrm{DIF}_{\mathrm{PR}}$	DIF _{FR} /
10 kN/m UDL							
t8-8.8-FT	91	47	1.94	77	46	1.67	1.17
t12-8.8-FT	82	43	1.93	76	42	1.80	1.07
t8-A4-80-FT	84	47	1.80	78	47	1.67	1.08
t12-A4-80-FT	84	44	1.92	78	43	1.81	1.06
t8-A4-80-PT	86	46	1.88	74	44	1.67	1.13
t12-A4-80-PT	78	46	1.72	74	44	1.71	1.01
t8-DX109-FT	85	47	1.81	77	47	1.64	1.10
t12-DX109-FT	87	46	1.88	79	44	1.78	1.06
20 kN/m UDL							
t8-8.8-FT	153	92	1.67	164	98	1.68	0.99
t12-8.8-FT	139	77	1.81	155	82	1.89	0.96
t8-A4-80-FT	154	89	1.72	169	94	1.80	0.96
t12-A4-80-FT	137	77	1.77	159	80	2.00	0.89
t8-A4-80-PT	153	88	1.74	154	97	1.58	1.10
t12-A4-80-PT	131	75	1.74	142	80	1.79	0.98
t8-DX109-FT	155	89	1.74	165	97	1.71	1.02
t12-DX109-FT	137	78	1.76	160	81	1.99	0.88

Table 8
Comparison of static and dynamic column removal results for TSWAC.

Model	F _{dy,FR} (kN)	F _{st,FR} (kN)	$\mathrm{DIF}_{\mathrm{FR}}$	F _{dy,PR} (kN)	F _{st,PR} (kN)	$\mathrm{DIF}_{\mathrm{PR}}$	DIF _{FR} /
10 kN/m UDL							
t8-8.8-FT	81	45	1.79	78	44	1.77	1.01
t12-8.8-FT	100	60	1.67	98	56	1.76	0.95
t8-A4-80-FT	83	47	1.76	84	45	1.84	0.95
t12-A4-80-FT	104	62	1.69	101	54	1.86	0.91
t8-A4-80-PT	90	43	2.08	83	44	1.88	1.11
t12-A4-80-PT	109	56	1.94	106	56	1.91	1.02
t8-DX109-FT	87	45	1.92	84	45	1.84	1.04
t12-DX109-FT	95	63	1.52	97	57	1.68	0.90
20 kN/m UDL							
t8-8.8-FT	121	61	1.98	124	62	2.00	0.99
t12-8.8-FT	162	104	1.56	163	80	2.05	0.76
t8-A4-80-FT	122	63	1.94	128	65	1.98	0.98
t12-A4-80-FT	162	85	1.90	166	80	2.06	0.92
t8-A4-80-PT	123	66	1.87	132	58	2.25	0.83
t12-A4-80-PT	153	86	1.78	159	79	2.01	0.89
t8-DX109-FT	128	63	2.03	131	67	1.95	1.04
t12-DX109-FT	152	91	1.67	157	85	1.85	0.90

to 2.0 as displacement demand increased, while for the TSWAC connections, it ranged from 1.7 to 2.2. These results indicate that the dynamic response of these connections was strongly influenced by their capability for plastic deformation. In early progressive collapse standards such as those from General Services Administration (GSA) [5] and the Department of Defense (DoD) [57], the DIF parameter was calibrated at 2.0. However, under high uniformly distributed loads (UDL), DIF values for the TSWAC connections exceeded this limit. This phenomenon has also been documented in other numerical investigations incorporating inelastic response considerations during column removal scenarios [58,59].

It is worth noting that the use of more ductile connections can mitigate the adverse effects of dynamic loading by increasing the system's energy absorption capacity. Higher ductility allows for greater plastic deformation before failure, enabling redistribution of internal forces and smoother force transitions. This plastic deformation mechanism acts as an energy dissipation source, effectively reducing peak dynamic responses and, consequently, the observed Dynamic Increase Factors (DIFs). The energy balance principle supports these observations. As the connection reaches its maximum dynamic displacement, the external work caused by sudden column removal must be balanced by the strain energy stored within the connection. If the energy dissipation capacity of the connection is insufficient—especially under higher UDLs and partial boundary constraints - a greater resisting force is required to maintain equilibrium. This results in DIF values that exceed the typical 2.0 threshold observed in our study. This discrepancy between expected and observed DIF values highlights the importance of considering dynamic effects in the design and assessment of structural connections. Izzuddin et al. [8] emphasized the need to account for dynamic impacts in progressive collapse scenarios. The dynamic behaviour of WA and TSWAC connections under sudden column removal shows significant differences from their static performance, particularly in terms of load capacity and energy absorption. In conclusion, the DIF values observed in this study highlight the increased demands on WA and TSWAC connections under dynamic loading, which are not fully captured by traditional static analysis, unless an appropriately high DIF is used. These results underscore the necessity of incorporating dynamic considerations into structural design to ensure resilience against progressive collapse. The findings from this analysis both confirm and extend previous research, demonstrating that both material properties and the geometric configuration of connections are critical to their dynamic performance.

5. Conclusions

This study explored the application of stainless steel angle cleats and bolts to enhance progressive collapse resistance in web angle (WA) and top-and-seat with web angle (TSWAC) connections. By replacing ductility-critical carbon steel components with high-ductility stainless steel, the objective was to improve connection performance under large deformations. Finite element simulations of unilateral connections and subframes under static and dynamic column-removal scenarios were conducted to assess the effects of loading types, bolt grades, angle thicknesses, and boundary conditions. The key findings are as follows:

- Stainless steel bolted-angle connections exhibited superior moment resistance and rotational ductility compared to carbon steel counterparts, due to their inherent strain hardening and ductility.
- Column removal analyses identified flexure, transition and catenary stages in load transfer. Thinner angles improved ductility and catenary action, while thicker ones increased stiffness. Stainless steel bolts and partially restrained conditions enhanced vertical load capacity and redistribution. Optimising these parameters is key to mitigating progressive collapse.
- Structural response under dynamic column removal was governed by UDL, restraints, angle thickness and bolt type. Higher UDLs led to larger displacements; full restraints limited deformation, while partial restraints enabled better redistribution. High-strength, ductile bolts (DX109, A4–80 PT) significantly reduced displacements compared to carbon steel bolts.
- Dynamic Increase Factors (DIFs) ranged from 1.7 to 2.0 for WA and 1.7–2.2 for TSWAC connections, highlighting the role of plastic deformation in force redistribution during sudden column loss. TSWAC connections under high UDLs exceeded the DIF limit, indicating higher force magnification and reduced ductility. These results stress the need to account for dynamic effects in design, as static analysis may underestimate demands, especially in stiffer systems.
- Overall, this research underscores the importance of selecting appropriate components, detailing, and integrating dynamic effects into the design process to ensure that connections meet both static and dynamic requirements. The study advocates for a balanced design approach that considers both stiffness and ductility to optimize connection performance and safety. The validated results enhance current design understanding and may inform future updates to design codes. Ongoing work will investigate strain rate effects and gradual column removal scenarios to further refine the understanding of connection robustness.

CRediT authorship contribution statement

Weiran Li: Writing – original draft, Validation, Methodology, Formal analysis, Data curation. **Manuela Cabrera:** Writing – original draft, Formal analysis, Data curation. **Marios Theofanous:** Writing – review & editing, Supervision, Funding acquisition, Conceptualization. **Sheida Afshan:** Writing – review & editing, Supervision, Project administration, Funding acquisition, Conceptualization.

Declaration of competing interest

None.

Acknowledgements

This research was conducted under the EPSRC project Resilient buildings using stainless steel (RESIST) with Grant Numbers P/W020351/1 and EP/W019809/1. The simulations were performed using the University of Southampton High Performance Computing (HPC) facility and the University of Birmingham's BlueBEAR HPC service which is gratefully acknowledge.

Data availability

Data will be made available on request.

References

- British Standards Institution, BS EN 1991-1-7, 2006 Eurocode 1: Actions on Structures – General Actions – Accidental Actions, British Standards Institution, 2006
- [2] J.M. Adam, F. Parisi, J. Sagaseta, X. Lu, Research and practice on progressive collapse and robustness of building structures in the 21st century, Eng. Struct. 173 (2018) 122–149.
- [3] B.R. Ellingwood, Mitigating risk from abnormal loads and progressive collapse, J. Perform. Constr. Facil. 20 (4) (2006) 315–323.
- [4] F. Kiakojouri, M.R. Sheidaii, V. De Biagi, B. Chiaia, Progressive collapse of structures: a discussion on annotated nomenclature, Structures 29 (2021) 1417–1423.
- [5] General Services Administration, Progressive Collapse Analysis and Design Guidelines for New Federal Office Buildings and Major Modernization Projects, GSA, 2003.
- [6] United States Department of Defense, Unified Facilities Criteria (UFC) 4–023-03: Design of Buildings to Resist Progressive Collapse, UFC, 2009.
- [7] American Society of Civil Engineers, Minimum Design Loads and Associated Criteria for Buildings and Other Structures, ASCE/SEI, 2022.
- [8] B. Izzuddin, A. Vlassis, A. Elghazouli, D. Nethercot, Progressive collapse of multistorey buildings due to sudden column loss—part I: simplified assessment framework, Eng. Struct. 30 (5) (2008) 1308–1318.
- [9] G. Gudmundsson, B. Izzuddin, The 'sudden column loss' idealisation for disproportionate collapse assessment, Struct. Eng. 88 (6) (2010) 22–26.
- [10] S. Gao, L. Guo, Progressive collapse analysis of 20-storey building considering composite action of floor slab, Int. J. Steel Struct. 15 (2015) 447–458.
- [11] J.M. Weigand, J.W. Berman, Integrity of bolted angle connections subjected to simulated column removal, J. Struct. Eng. 142 (3) (2016), 04015165.
- [12] D. Cassiano, M. D'Aniello, C. Rebelo, Parametric finite element analyses on flush end-plate joints under column removal, J. Constr. Steel Res. 137 (2017) 77–92.
- [13] K. Chen, K.H. Tan, Composite joints with fin plate connections under a middle column removal scenario, J. Constr. Steel Res. 161 (2019) 258–274.
- [14] M. Byfield, S. Paramasivam, Catenary action in Steel-framed buildings, Proc. Inst. Civ. Eng.-Struct. Build. 160 (5) (2007) 247–257.
- [15] B. Yang, K.H. Tan, Behavior of composite beam-column joints in a middle-column-removal scenario: experimental tests, J. Struct. Eng. 140 (2) (2014) 04013045.
- [16] F. Xie, B. Gu, H. Qian, Experimental study on the dynamic behavior of steel frames during progressive collapse, J. Constr. Steel Res. 177 (2021) 106459.
- [17] B. Yang, K.H. Tan, Experimental tests of different types of bolted steel beam-column joints under a central-column-removal scenario, Eng. Struct. 54 (2013) 112–130.
- [18] F. Sadek, J.A. Main, H.S. Lew, S.D. Robert, V.P. Chiarito, S. El-Tawil, An experimental and computational study of steel moment connections under a column removal scenario, NIST Technical Note 1669 (2010).
- [19] G. Bregoli, G. Vasdravellis, T.L. Karavasilis, D.M. Cotsovos, Static and dynamic tests on steel joints equipped with novel structural details for progressive collapse mitigation, Eng. Struct. 232 (2021) 111829.
- [20] B. Yang, K.H. Tan, Robustness of bolted-angle connections against progressive collapse: experimental tests of beam-column joints and development of component-based models, J. Struct. Eng. 139 (9) (2013) 1498–1514.
- [21] T. Kim, J. Kim, J. Park, Investigation of progressive collapse-resisting capability of steel moment frames using push-down analysis, J. Perform. Constr. Facil. 23 (5) (2009) 327–335.
- [22] P. Stylianidis, D. Nethercot, Modelling of connection behaviour for progressive collapse analysis, J. Constr. Steel Res. 113 (2015) 169–184.
- [23] P. Stylianidis, D. Nethercot, B. Izzuddin, A. Elghazouli, Robustness assessment of frame structures using simplified beam and grillage models, Eng. Struct. 115 (2016) 78–95.
- [24] V.R. Gomes, A. Tenchini, L. Lima, P. Vellasco, Robustness assessment of semi-rigid steel multi-storey frames, Structures 25 (2020) 849–860.
- [25] K. Khandelwal, S. El-Tawil, S.K. Kunnath, H. Lew, Macromodel-based simulation of progressive collapse: steel frame structures, J. Struct. Eng. 134 (7) (2008) 1070–1078.
- [26] H.Z. Jahromi, A. Vlassis, B. Izzuddin, Modelling approaches for robustness assessment of multi-storey steel-composite buildings, Eng. Struct. 51 (2013) 278–294.
- [27] S. Afshan, L. Gardner, The continuous strength method for structural stainless steel design, Thin-Walled Struct. 68 (2013) 42–49.
- [28] L. Gardner, Stability and design of stainless steel structures-review and outlook, Thin-Walled Struct. 141 (2019) 208–216.
- [29] A. Pournaghshband, S. Afshan, A. Foster, Structural fire performance of axially and rotationally restrained stainless steel columns, Thin-Walled Struct. 137 (2019) 561–572.
- [30] M.A. Shaheen, A.S. Foster, L.S. Cunningham, S. Afshan, A numerical investigation into stripping failure of bolt assemblies at elevated temperatures, Structures 27 (2020) 1458–1466.
- [31] M. Elflah, M. Theofanous, S. Dirar, H. Yuan, Behaviour of stainless steel beam-to-column joints—part 1: experimental investigation, J. Constr. Steel Res. 152 (2019) 183–193.

- [32] Y. Song, J. Wang, B. Uy, D. Li, Stainless steel bolts subjected to combined tension and shear: behaviour and design, J. Constr. Steel Res. 170 (2020) 106122.
- [33] Y. Song, J. Wang, B. Uy, D. Li, Experimental behaviour and fracture prediction of austenitic stainless steel bolts under combined tension and shear, J. Constr. Steel Res. 166 (2020) 105916.
- [34] British Standards Institution, EN 1993-1-8:2024 Eurocode 3: Design of Steel Structures – Part 1–8: Design of Joints. Annex C: Component method for bolted beam-to-column connections, British Standards Institution, CEN, 2024.
- [35] X. Yun, L. Gardner, Stress-strain curves for hot-rolled steels, J. Constr. Steel Res. 133 (2017) 36–46.
- [36] K.J. Rasmussen, Full-range stress-strain curves for stainless steel alloys, J. Constr. Steel Res. 59 (1) (2003) 47–61.
- [37] E. Mirambell, E. Real, On the calculation of deflections in structural stainless steel beams: an experimental and numerical investigation, J. Constr. Steel Res. 54 (1) (2000) 109–133
- [38] M. Elflah, M. Theofanous, S. Dirar, Behaviour of stainless steel beam-to-column joints-part 2: numerical modelling and parametric study, J. Constr. Steel Res. 152 (2019) 194–212.
- [39] A. Kanvinde, G. Deierlein, The void growth model and the stress modified critical strain model to predict ductile fracture in structural steels, J. Struct. Eng. 132 (12) (2006) 1907–1918
- [40] J.R. Rice, D.M. Tracey, On the ductile enlargement of voids in triaxial stress fields*, J. Mech. Phys. Solids 17 (3) (1969) 201–217.
- [41] G. Rousselier, Ductile fracture models and their potential in local approach of fracture, Nucl. Eng. Des. 105 (1) (1987) 97–111.
- [42] Abaqus Analysis User"s Guide, Dassault Syst'emes Simulia Corp., Providence, RI, USA, 2023.
- [43] SolidWorks (Version 2022), SolidWorks Corporation., Waltham, MA, USA, 2022.
- [44] O. Yapici, M. Theofanous, S. Afshan, H. Yuan, S. Dirar, Numerical modelling of stainless steel bolted T-stubs in tension, Thin-Walled Struct. 177 (2022) 109432.
- [45] L. Luo, M. Du, J. Yuan, J. Shi, S. Yu, Y. Zhang, Parametric analysis and stiffness investigation of extended end-plate connection, Materials 13 (22) (2020) 5133.

- [46] A.K. Chopra, Dynamics of Structures: Theory and Applications to Earthquake Engineering, fourth ed, Prentice Hall, Upper Saddle River, NJ, 2012.
- [47] SCI, Joints in Steel Construction: Simple Joints to Eurocode 3, The Steel Construction Institute, Ascot, 2011.
- [48] F. Yang, M. Veljkovic, Y. Liu, Fracture simulation of partially threaded bolts under tensile loading, Eng. Struct. 226 (2021) 111373.
- [49] N. Stranghöner, C. Abraham, Tension and interaction resistance of austenitic and duplex stainless steel bolts, J. Constr. Steel Res. 198 (2022) 107536.
- [50] H. Yuan, S. Hu, X. Du, L. Yang, X. Cheng, M. Theofanous, Experimental behaviour of stainless steel bolted T-stub connections under monotonic loading, J. Constr. Steel Res. 152 (2019) 213–224.
- [51] H. Yuan, J. Gao, M. Theofanous, L. Yang, B. Schafer, Initial stiffness and plastic resistance of bolted stainless steel T-stubs in tension, J. Constr. Steel Res. 173 (2020) 106239.
- [52] Y. Ling, Uniaxial true stress-strain after necking, AMP J. Technol. 5 (1) (1996) 37–48.
- [53] Y. Bao, T. Wierzbicki, A comparative study on various ductile crack formation criteria, J. Eng. Mater. Technol. 126 (3) (2004) 314–324.
- [54] Y. Lee, T. Wierzbicki, Quick Fracture Calibration for Industrial Use, Report no: 115, Impact and Crashworthiness Laboratory, Massachusetts Institute of Technology, 2004
- [55] British Standards Institution, BS EN, Eurocode 3: Design of Steel Structures Part 1–8: Design of Joints, British Standards Institution, CEN, 2005.
- [56] A. Elkady, Response characteristics of flush end-plate connections, Eng. Struct. 269 (2022) 114856.
- [57] United States Department of Defense, Unified Facilities Criteria (UFC) 4-023-03: Design of Buildings to Resist Progressive Collapse, UFC, 2004.
- [58] M.-H. Tsai, An analytical methodology for the dynamic amplification factor in progressive collapse evaluation of building structures, Mech. Res. Commun. 37 (1) (2010) 61–66.
- [59] H.-S. Kim, J. Kim, D.-W. An, Development of integrated system for progressive collapse analysis of building structures considering dynamic effects, Adv. Eng. Softw. 40 (1) (2009) 1–8.